


Research Article

In Situ Preparation and Properties of Poly(vinyl alcohol)/Carboxymethyl Chitosan/Cyanidin Hydrogel Films

Xiaojuan Zhang ^{1,2}, Wenbin Cai^{1,2}, Lingyun Hao ^{1,2} and Wei Zhang^{1,2,3}

¹School of Material Engineering, Jinling Institute of Technology, Nanjing 211169, China

²Nanjing Key Laboratory of Optometric Materials and Technology, Nanjing 211169, China

³College of Mechanics and Materials, Hohai University, Nanjing 211100, China

Correspondence should be addressed to Lingyun Hao; hly_jit@163.com

Received 21 August 2018; Revised 11 December 2018; Accepted 4 February 2019; Published 27 March 2019

Academic Editor: Ilaria Fratoddi

Copyright © 2019 Xiaojuan Zhang et al. This is an open access article distributed under the Creative Commons Attribution License, which permits unrestricted use, distribution, and reproduction in any medium, provided the original work is properly cited.

This study synthesized poly(vinyl alcohol)/carboxymethyl chitosan/cyanidin (PVA/CMCS/CY) hydrogel films. First, PVA and CMCS were used to synthesize hydrogel films by ultraviolet irradiation. Meanwhile, CY was in situ combined into the hydrogel films through the electrostatic attraction between CMCS and CY. Next, the products were analyzed using Fourier-transform infrared spectroscopy, scanning electron microscopy, contact angle test, swelling analysis, and mechanical property test. The results revealed that compared with PVA/CMCS hydrogel films, the PVA/CMCS/CY hydrogel films had an interporous structure and good swelling and mechanical properties. Moreover, the drug release experiments demonstrated that the PVA/CMCS/CY hydrogel films had a CY encapsulation efficiency of 33.5% with a sustained CY release of up to 60 h. Furthermore, the examined antibacterial activities against *Staphylococcus aureus* and *Escherichia coli* showed that the porous PVA/CMCS/CY hydrogel films exhibited a certain inhibition. Cell viability experiments demonstrated that the PVA/CMCS/CY films displayed no obvious cytotoxicity to human umbilical vein endothelial cells.

1. Introduction

Cyanidin (CY) is an anthocyanin (ATC) that belongs to flavonoids and is found in fruits, vegetables, and flowers [1]. In recent years, CY has been extensively studied because of its α -glucosidase inhibitory, antioxidative, anti-inflammatory, antibacterial, and antitumor properties [2–6]. However, due to its insufficient absorption and short half-life in vivo metabolism, its clinical application is limited [7, 8]. To improve its absorption, CY has been loaded into different carriers, such as gelling systems [9], poly(lactide-co-glycolide)/polyethylene glycol (PEG) nanoparticles [10], liposomes [11], chitosan-cellulose microcapsules [12], cyclodextrin [13], ferritin nanocage [14], chitosan nanoparticles [15], and chitosan/PVA films [16]. The combination of CY into different materials will support the development of multifunctional drug delivery. For instance, Jeong et al. [17] prepared a chondroitin sulfate-(CS-) ATC nanocomplex and loaded doxorubicin (DOX) into the nanocomplex through an intermolecular stacking

interaction. Their results showed that the CS-ATC2-DOX nanocomplex exhibited a reactive-oxygen-species-sensitive therapeutic effect and inhibited tumor growth. Kim et al. [18] synthesized ATC-loaded PEG-gold nanoparticles, which achieved an enhanced delivery of ATC in the mouse brain and could prevent neurodegenerative diseases.

Hydrogel is a three-dimensional network polymeric material containing water or biological substances, which can be applied in drug delivery, regenerative medicine, and wound dressing [19]. There are various types of hydrogel wound dressing materials, including poly(vinyl alcohol) (PVA), chitosan, alginate, nanofibrillar cellulose, and gelatin [20, 21]. Sung et al. used the freeze-thaw method to prepare a minocycline-loaded PVA/CS hydrogel wound dressing, which displayed an excellent swelling ability, elasticity, form, and enhanced wound healing [22]. Swaroop et al. [23] used gamma irradiation to synthesize a PVA/Ag hydrogel with good swelling rate (SR) and antibiotic property for wound dressing. Chitosan hydrogel films and membranes have been widely applied in wound dressing. Chitosan does not exhibit

any antibacterial activity at neutral pH. To impart the antibacterial properties of hydrogels, drugs were loaded into hydrogel films. For instance, Kumar et al. [24] prepared flexible and microporous CS/ZnO composite hydrogel films with enhanced swelling, blood clotting, antibacterial activity, and good biocompatibility. Singh and Pal [25] synthesized PVA/poly(AAm) hydrogel films loaded with tetracycline and gentamicin by sterculia crosslinking, which significantly improved the wound healing effect.

In this study, the antibacterial CY was introduced into PVA/CMCS hydrogel films through in situ ultraviolet (UV) irradiation, and the properties of PVA/CMCS/CY were examined. Furthermore, the biocompatibility of PVA/CMCS/CY on human umbilical vein endothelial cells (HUVECs) was investigated.

2. Experimental

2.1. Materials. PVA was procured from Aladdin. Carboxymethyl chitosan (CMCS), acrylic acid (AA), phosphate buffer (PBS), cyanidin chloride (CY), *Escherichia coli* (*E. coli*), *Staphylococcus aureus* (*S. aureus*), Luria–Bertani (LB) agar, and drug-sensitive papers (streptomycin and cefixime) were purchased from Sinopharm Chemical Reagent Co. Ltd. Distilled water from a Millipore-Q system was used as the solvent.

2.2. Synthesis of PVA/CMCS/CY Hydrogel Films. The synthesis of the PVA/CMCS/CY hydrogel films is shown in Figure 1. CY was in situ incorporated into the PVA/CMCS hydrogel network through an electrostatic attraction between CMCS and CY. First, 0.4 g of CMCS and 0.0022 g of CY were dispersed into 38.6 mL of H₂O. Then, 1.0 g of PVA was added into the solution at 90°C for 2 h with stirring. After the mixture was cooled to 50°C, 2.5 mL of AA was added. Subsequently, the solution containing PVA, CMCS, CY, and AA was cast onto glass slides and exposed to a UV lamp at room temperature for 10 h under N₂. The resultant hydrogel films were collected from the slides and extracted in deionized water at 50°C for 48 h. Finally, the PVA/CMCS/CY hydrogel films were vacuum-dried at 40°C for 24 h. For comparison, we synthesized PVA/CMCS hydrogel films without adding CY.

2.3. Determination of the Infrared (IR) Spectrum, Scanning Electron Microscopy (SEM) Morphology, and Contact Angles of the Hydrogel Films. The Bruker Vector 22 spectrometer was used to measure the IR spectrum of hydrogel films. The films' morphology was measured by SEM (Model S-4800). The contact angles of the hydrogel films were tested using a contact angle meter (Kruss DSA25, Germany).

2.4. Swelling Properties of the Hydrogel Films. The SR was measured in PBS (pH 7.4) at different temperatures: (a) 25°C, (b) 37°C, and (c) 40°C. The PVA/CMCS and PVA/CMCS/CY hydrogel films (2 cm × 2 cm) were dispersed in 100 mL of PBS solution at different temperatures for 24 h

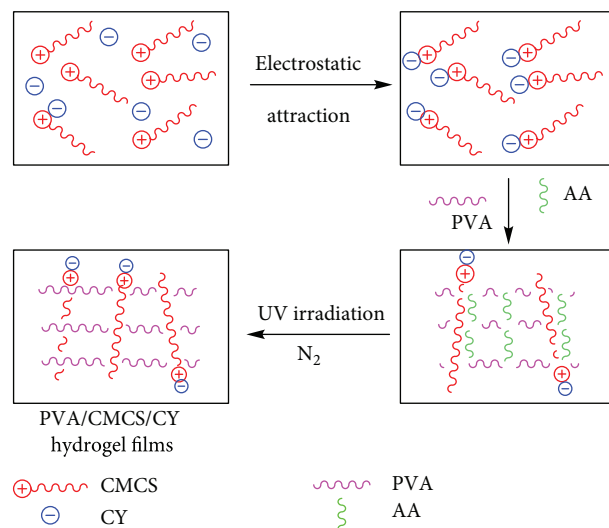


FIGURE 1: Schematic of the formation processes of PVA/CMCS/CY hydrogel films.

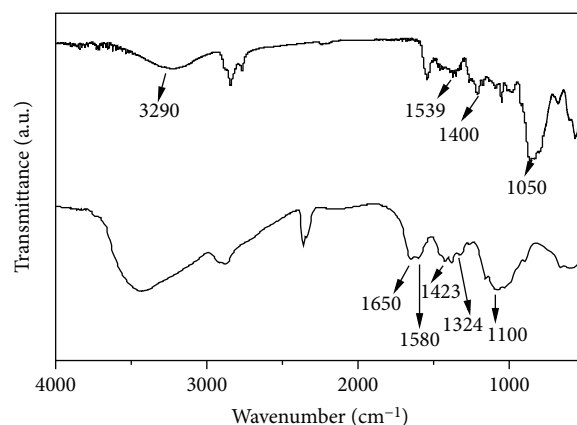


FIGURE 2: FT-IR spectra of (a) PVA/CMCS and (b) PVA/CMCS/CY hydrogel films.

to reach the maximum swelling equilibrium. The SR of the hydrogel films was determined using the following [26]:

$$SR = \frac{(w_2 - w_1)}{w_1} \times 100\%, \quad (1)$$

where w_1 is the initial mass of the sample and w_2 is the mass of the sample after swelling for 24 h.

2.5. Mechanical Properties of the Hydrogel Films. The tensile strength and elongation at break of the PVA/CMCS and PVA/CMCS/CY hydrogel films were tested using a universal testing machine (Instron, Model 5943), and the cross-head speed was 20 mm/min at room temperature. The PVA/CMCS hydrogel films were prepared with dimensions of 15 mm × 9.5 mm × 0.1285 mm, and the PVA/CMCS/CY hydrogel films were cut with dimensions of 15 mm × 9.9 mm × 0.077 mm.

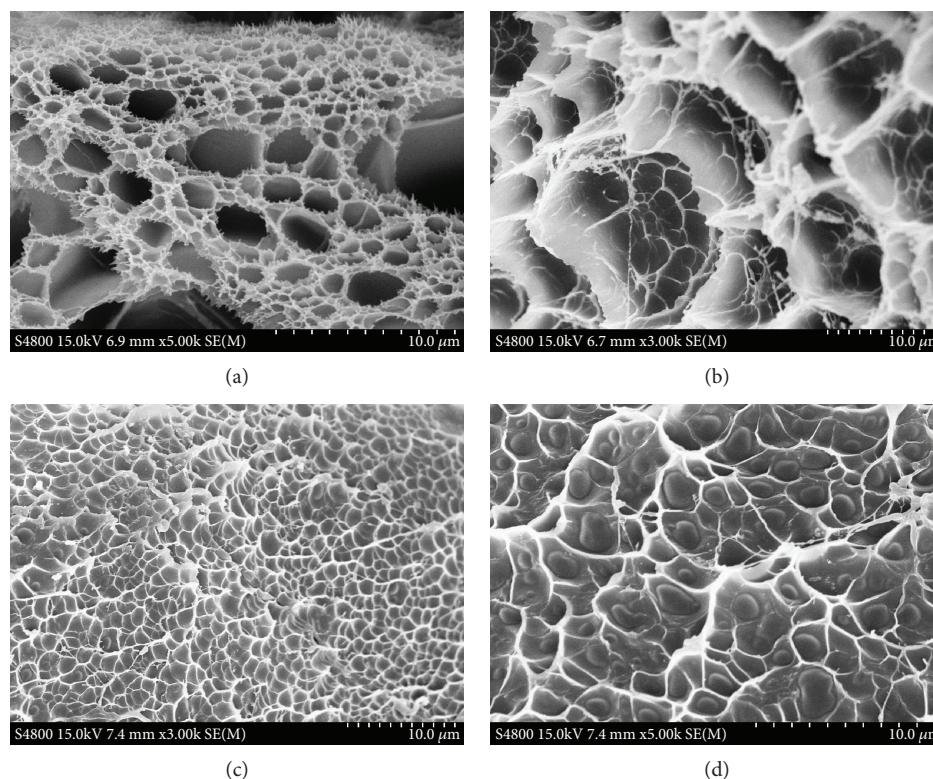


FIGURE 3: SEM images of (a, b) PVA/CMCS and (c, d) PVA/CMCS/CY hydrogel films.

2.6. Drug Release of the PVA/CMCS/CY Hydrogel Films. The release of PVA/CMCS/CY was tested in pH = 5.5 (mimicking the endosome pH) and pH = 7.4 (simulated body fluid) so as to speculate whether acidic conditions could influence the release behaviors or not. Approximately 10 mg of PVA/CMCS/CY was suspended in a conical flask containing 50 mL buffer and was kept in a shaking incubator at 37°C and 95 rpm. The incubated solution (3 mL) was collected and replaced with an equal volume of buffer. The CY release was characterized by an UV-visible spectrophotometer (UV1101M054) at 282 nm. The encapsulation and drug loading efficiencies were calculated using equations (2) and (3), respectively, as follows:

$$\text{Encapsulation efficiency} = \frac{m_d}{m_0} \times 100\%, \quad (2)$$

$$\text{Drug loading efficiency} = \frac{m_d}{m_t} \times 100\%, \quad (3)$$

where m_d is the mass of CY in the PVA/CMCS/CY hydrogel films, m_t is the total mass of the PVA/CMCS/CY hydrogel films, and m_0 is the total mass of CY.

2.7. Antibacterial Study of the PVA/CMCS/CY Hydrogel Films. The antibacterial activity of the prepared PVA/CMCS/CY hydrogel films was evaluated against *E. coli* and *S. aureus*. LB agar was used as the culture medium. The PVA/CMCS/CY hydrogel films, the PVA/CMCS hydrogel films, and the drug-sensitive papers (streptomycin and cefixime) were spread on the culture medium, which was evenly coated with

bacteria. After 24 h of culture, the antibacterial effect was measured based on the inhibition zone surrounding each sample.

2.8. In Vitro Cytotoxicity of the PVA/CMCS/CY Hydrogel Films. HUVECs were selected to measure the cytotoxicity of PVA/CMCS/CY hydrogel films by using 3-(4,5-dimethylthiazol-2-yl)-2,5-diphenyltetrazolium bromide (MTT) assay [27]. Approximately 200 μ L of HUVEC was seeded into a 96-well plate. Different concentrations of PVA/CMCS/CY (0.5, 1, 10, and 50 μ g/mL) were added to each group (six wells) for 24 h. The absorbance was measured at a wavelength of 490 nm by using the Multiskan FC enzyme-labeled instrument (Thermo Scientific, USA). In addition, the number of viable cells was measured on day 3 by fluorescence microscopy (Olympus CKX41).

3. Results and Discussion

3.1. Fourier-Transform Infrared (FT-IR) Analysis. The FT-IR spectra for PVA/CMCS and PVA/CMCS/CY hydrogel films are shown in Figure 2, a and b, respectively. In Figure 2(a), C=O amide stretching vibration peaks appeared at 1650 cm^{-1} . The peaks at 1580, 1423, 1324, and 1100 cm^{-1} could be ascribed to the absorption of the amide group, CH-OH bending, C-H bond, and C-C backbone, respectively [28]. This result indicated that PVA and CMCS were successfully cross-linked to form a hydrogel. In Figure 2(b), the peaks at 3290, 1539, 1400, and 1050 cm^{-1} could be attributed to the O-H, benzene ring, C-O bending, and C-O-C of CY, which indicated that CY was loaded into PVA/CMCS hydrogel films.

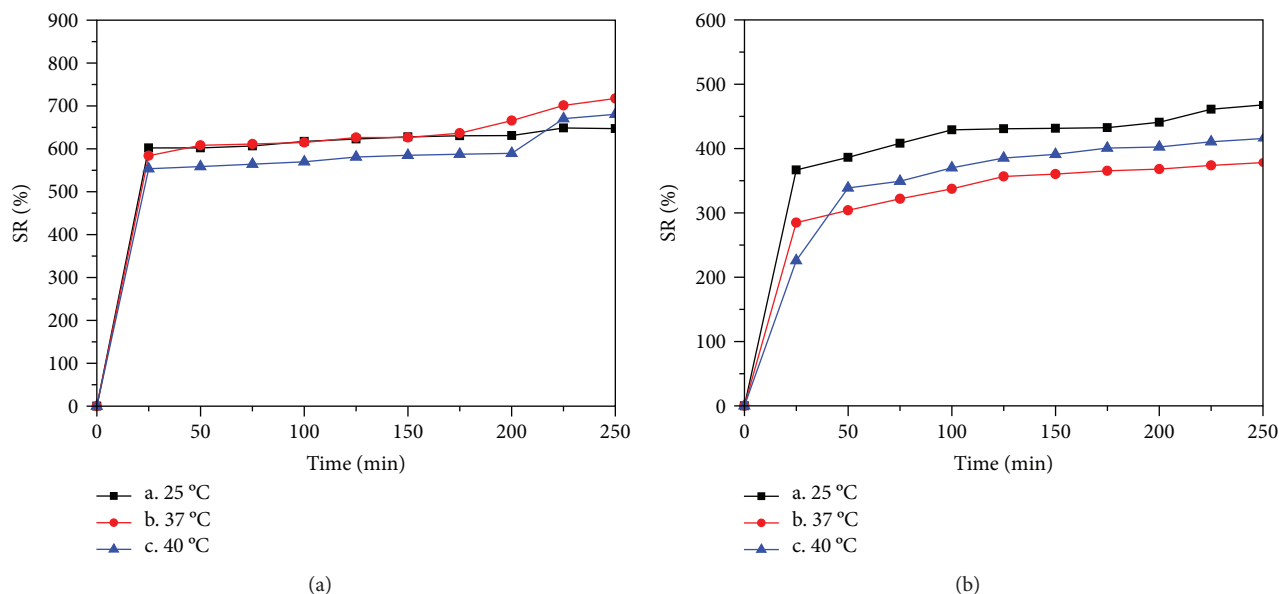


FIGURE 4: SRs of PVA/CMCS (a) and PVA/CMCS/CY hydrogel films in PBS (pH 7.4) and at different temperatures: (a) 25°C, (b) 37°C, and (c) 40°C.

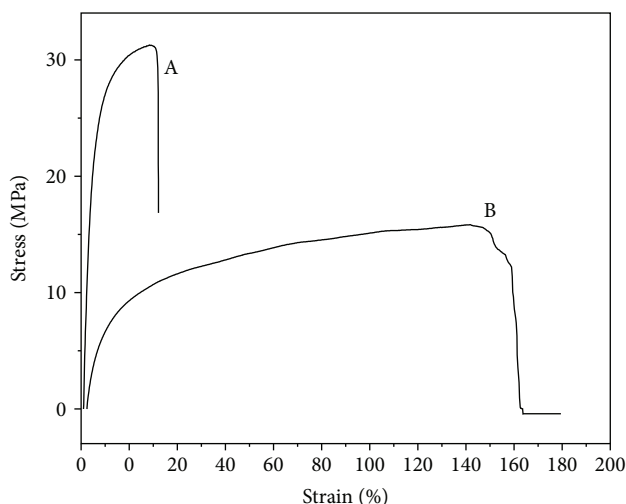


FIGURE 5: Typical tensile stress-strain curves of (a) PVA/CMCS and (b) PVA/CMCS/CY hydrogel films determined at room temperature.

3.2. SEM Analysis. The SEM images of PVA/CMCS and PVA/CMCS/CY hydrogel films are shown in Figure 3. As shown in Figure 3(a), the surface of PVA/CMCS hydrogel films displayed a honeycomb-like structure with interconnecting pores. As shown in Figure 3(b), the pore sizes of the network were in the range of several micrometers. Figures 3(c) and 3(d) show that the PVA/CMCS/CY hydrogel films exhibited a 3D porous network structure [29], and the addition of CY obviously affected the interior morphology of the hydrogel. The addition of CY led to a compact interior structure and small pores of the PVA/CMCS/CY hydrogel films. The pore size decreased correspondingly with the concentration of CY increasing due to the decrease in the distance between the polymer chains and the increase of crosslink density. Besides, the decrement of the pore size

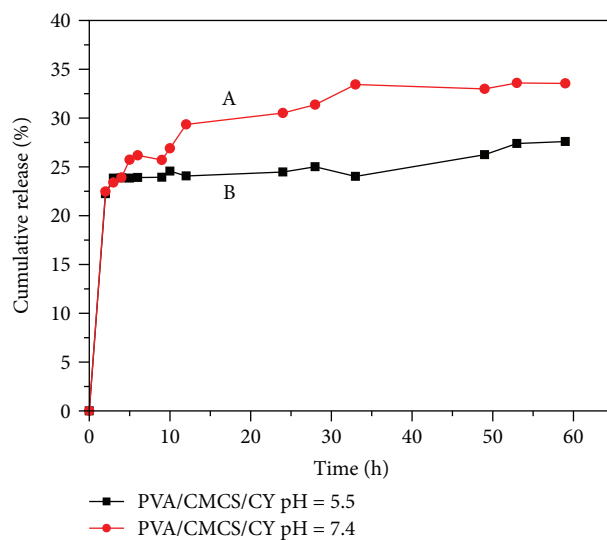


FIGURE 6: Release behavior of CY from PVA/CMCS/CY at (a) pH 7.4 and (b) pH 5.5.

may be attributed to the CY solution entering into the inner side of the sample through these interconnected pores by capillary force [30].

3.3. Contact Angle Analysis. The contact angles of the PVA/CMCS and PVA/CMCS/CY hydrogel films were $48.2^\circ \pm 0.9^\circ$ and $55.0^\circ \pm 1.2^\circ$, respectively. The contact angle of the PVA/CMCS/CY hydrogel films was higher than that of the PVA/CMCS films, indicating that the PVA/CMCS/CY hydrogel films were more hydrophobic than the PVA/CMCS films because of the presence of CY [30].

3.4. Analysis of Swelling Properties. Figures 4(a) and 4(b) show the SRs of the PVA/CMCS and PVA/CMCS/CY hydrogel films, respectively, in PBS (pH 7.4) and at different

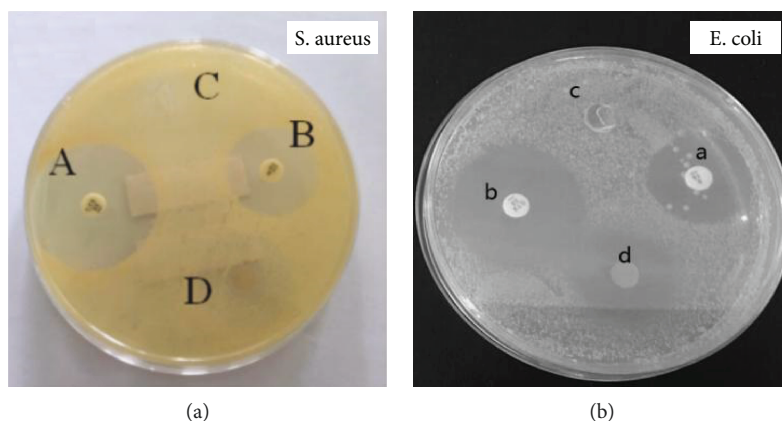


FIGURE 7: Antibacterial activity screening images of samples against (a) *S. aureus* and (b) *E. coli*: (A) streptomycin (S_{10}), (B) cefotaxime (CTX_{30}), (C) PVA/CMCS hydrogel films, and (D) PVA/CMCS/CY hydrogel films.

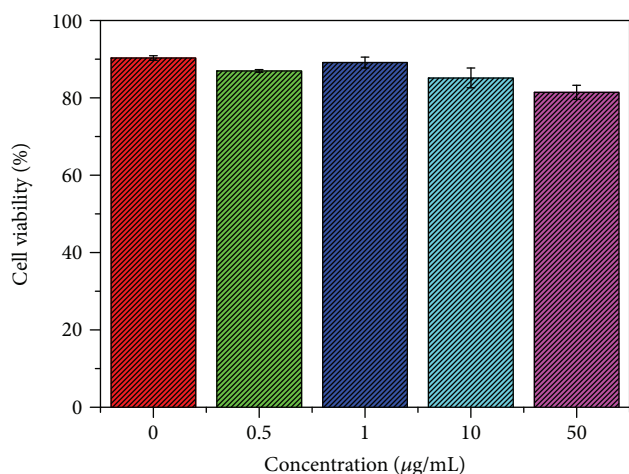


FIGURE 8: Histogram of cell viability as a function of PVA/CMCS/CY concentration in culture media.

temperatures: (a) 25°C, (b) 37°C, and (c) 40°C. All of the hydrogel films had a high swelling ratio due to CMCS and PVA having many hydrophilic groups. In Figure 4(a), the equilibrium SR of PVA/CMCS at 37°C reached up to 716% at 250 min, which was higher than that of PVA/CMCS at 25°C (645%) and 40°C (680%). Therefore, the swelling properties of the PVA/CMCS hydrogel films were beneficial for wound dressing application [31]. As shown in Figure 4(b), the SRs of the PVA/CMCS/CY hydrogel films were 467% (a, 25°C), 380% (b, 37°C), and 415% (c, 40°C). The decrease in the PVA/CMCS/CY hydrogel films may be attributed to the binding between CY and CMCS, which are responsible for higher cross-links. Compared with the PVA/CMCS hydrogel films, the higher cross-links restricted the water penetration for swelling. Moreover, the swelling ratio obviously decreased with the addition of CY, because the electrostatic attraction between CMCS and CY could limit the swelling force. Besides, the swelling ratio of the PVA/CMCS/CY hydrogel films was limited, which was attributed to that there were a lot of hydrogen bonds formed from CY and PVA ($-\text{OH}$ and $-\text{OH}$) and CY and CMCS ($-\text{OH}$ and $-\text{COOH}$).

3.5. Analysis of Mechanical Properties. The tensile tests provided an indication of the strength and elasticity of the hydrogel films, and the results suggested that the hydrogel films applied in wound dressing were strong yet flexible [32]. The mechanical properties of the PVA/CMCS and PVA/CMCS/CY hydrogel films are presented in Figure 5. As shown in Figure 5(a), PVA/CMCS had a tensile strength of 31.13 MPa and an elongation at break of 27.36%. As shown in Figure 5(b), the PVA/CMCS/CY hydrogel films exhibited a higher elongation at break (167.04%) but lower tensile strength (15.82 MPa) than the PVA/CMCS hydrogel films. These results indicated that PVA/CMCS/CY was softer and more flexible than the PVA/CMCS hydrogel films. Therefore, the addition of CY into the polymeric network could facilitate the rearrangement of molecular chains in composite films [28].

3.6. UV Analysis. The release profiles of CY from PVA/CMCS/CY are shown in Figure 6. The standard curve of CY can be derived using equation (4). The drug loading and encapsulation efficiencies of PVA/CMCS/CY were 17.3% and 33.5%, respectively.

$$A = 56.4972 \cdot C + 0.1695, \quad (4)$$

$$R^2 = 0.981.$$

In Figure 6, the PVA/CMCS/CY hydrogel films exhibited a severe burst release, and more than 22% CY was released in the first 2 h, which could be due to the attachment of the drugs to the surface of the hydrogel films. Approximately 33.5% (Figure 6(a)) and 27.6% (Figure 6(b)) of CY were released at pH 7.4 and 5.5 after 60 h, respectively. Therefore, the addition of CY resulted in the compact network structure of the PVA/CMCS/CY hydrogel, so the drug stored in the hydrogel films needed to be diffused by more polymer layers. Under a weak alkaline condition (pH = 7.4), the carboxylic acid groups in PVA/CMCS/CY hydrogel films were gradually ionized into carboxylate ions ($-\text{COO}^-$), which generate electrostatic repulsion to make the hydrogel films release fast. However, at an acidic condition (pH = 5.5), the electrostatic

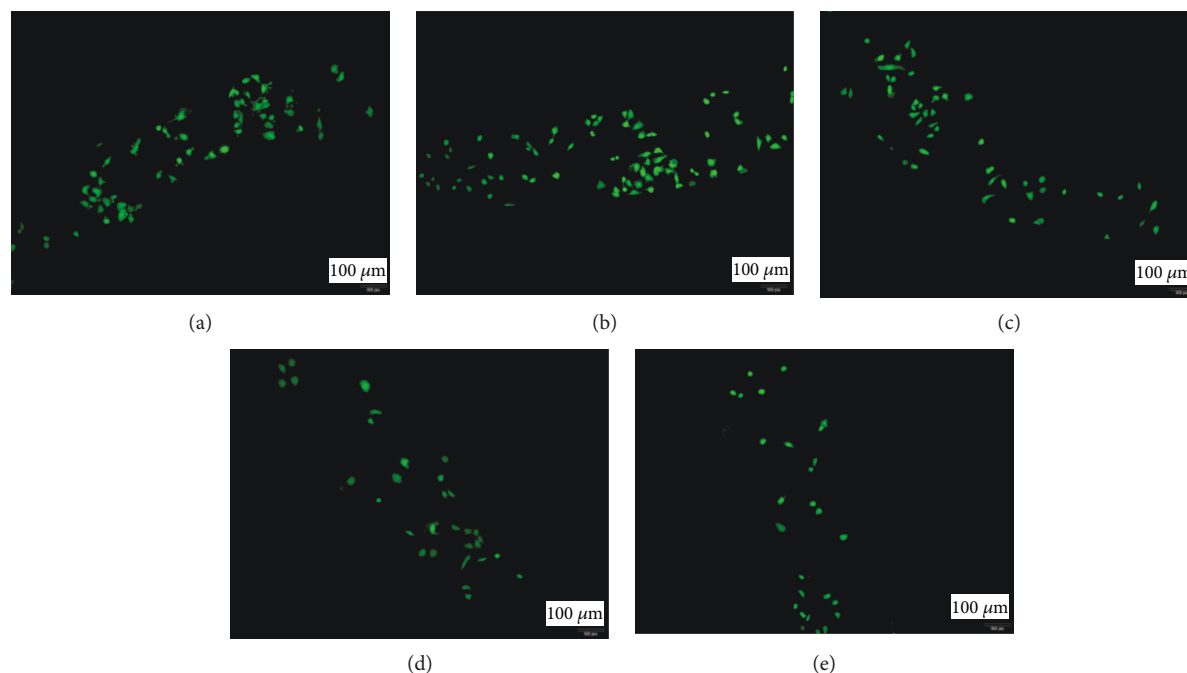


FIGURE 9: HUVECs observed by fluorescence microscopy on (a) the control and (b–e) the PVA/CMCS/CY hydrogel films of (b) 0.5 $\mu\text{g/mL}$, (c) 1 $\mu\text{g/mL}$, (d) 10 $\mu\text{g/mL}$, and (d) 50 $\mu\text{g/mL}$.

attraction from the protonation of amino groups ($-\text{NH}_3^+$) and CY could limit the drug release of hydrogel films. Moreover, in $\text{pH} = 5.5$, the protonation of amino groups on CMCS caused the breakage of the dynamic Schiff base linkage and thus increased the connectivity of internal pores of hydrogel films and limited the drug release.

3.7. Antibacterial Properties. The *in vitro* antibacterial potentials of (A) streptomycin (S_{10}), (B) cefotaxime (CTX_{30}), (C) PVA/CMCS, and (D) PVA/CMCS/CY hydrogel films were investigated for positive *S. aureus* (Figure 7(a)) and negative *E. coli* (Figure 7(b)) through the disc diffusion method. Streptomycin, cefotaxime, and PVA/CMCS/CY (Figure 7(a) (A, B, and D) and Figure 7(b) (A, B, and D)) expressed an inhibition zone, whereas the PVA/CMCS hydrogel films (Figures 7(a) (C) and Figure 7(b) (C)) did not possess an antibacterial activity. The control cefotaxime displayed an inhibition ring size of 9.3 and 14.3 mm for *S. aureus* and *E. coli*, respectively. The control streptomycin exhibited an inhibition ring size of 12.4 and 11.2 mm for *S. aureus* and *E. coli*, respectively. The PVA/CMCS/CY hydrogel films showed a growth inhibition ring size of 10.3 and 10.2 mm for *S. aureus* and *E. coli*, respectively. The PVA/CMCS/CY hydrogel films showed good antibacterial activities on both positive *S. aureus* and negative *E. coli*. The good antibacterial activity of the PVA/CMCS/CY hydrogel films could be attributed to the efficient release of CY in the media.

3.8. In Vitro Cytotoxicity Assay. Cell viability data (Figure 8) indicated that the PVA/CMCS/CY hydrogel films had no considerable cytotoxicity to HUVECs. The PVA/CMCS/CY hydrogel films with different concentrations achieved 90%–95% viability after 24 h of incubation. The cell viability results

of the products were further confirmed by fluorescence microscopy. The control group contained the largest number of viable cells (Figure 9(a)). With the addition of different concentrations of PVA/CMCS/CY (0.5, 1, 10, and 50 $\mu\text{g/mL}$, Figures 9(b)–9(e), respectively), HUVECs displayed no obvious morphological change. The PVA/CMCS/CY hydrogel films showed good biocompatibility for HUVECs, indicating their suitability for wound healing.

4. Conclusions

CY was successfully introduced into PVA/CMCS hydrogel films by *in situ* UV irradiation, and the effects of CY on the structure and properties were studied. The SEM images illustrated that the addition of CY resulted in the compact interior structure and small pores of the PVA/CMCS/CY hydrogel films. The tensile test indicated that the inclusion of CY within PVA/CMCS hydrogel networks improved the elasticity of the composite films. Moreover, the developed PVA/CMCS/CY hydrogel films showed good antibacterial activities against *S. aureus* and *E. coli*. Therefore, PVA/CMCS/CY nanocomposites have a promising application potential in wound dressing.

Data Availability

The data used to support the findings of this study are available from the corresponding author upon request.

Conflicts of Interest

The authors declare that they have no conflict of interest.

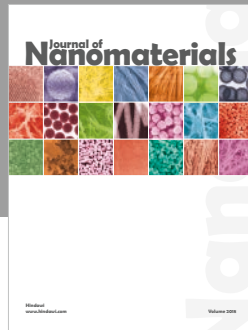
Acknowledgments

This work was supported by the sponsorship of the incentive projects of Jinling Institute of Technology (no. Jit-fhxm-201806), the research grants from Six Talent Peaks Project in Jiangsu Province (no. XCL-109), the Scientific and Technological Innovation Project for Overseas Teachers in Nanjing, the National Natural Science Foundation of China (61804069), and the sponsorship of Nanjing Key Laboratory of Optometric Materials and Technology.

References

- [1] T. Suantawee, H. Cheng, and S. Adisakwattana, "Protective effect of cyanidin against glucose- and methylglyoxal-induced protein glycation and oxidative DNA damage," *International Journal of Biological Macromolecules*, vol. 93, pp. 814–821, 2016.
- [2] S. Akkarachiyasit, P. Charoenlertkul, S. Yibchok-anun, and S. Adisakwattana, "Inhibitory activities of cyanidin and its glycosides and synergistic effect with acarbose against intestinal α -glucosidase and pancreatic α -amylase," *International Journal of Molecular Sciences*, vol. 11, no. 9, pp. 3387–3396, 2010.
- [3] P. Y. Chao, Y. P. Huang, and W. B. Hsieh, "Inhibitive effect of purple sweet potato leaf extract and its components on cell adhesion and inflammatory response in human aortic endothelial cells," *Cell Adhesion & Migration*, vol. 7, no. 2, pp. 237–245, 2013.
- [4] L. R. Fukumoto and G. Mazza, "Assessing antioxidant and prooxidant activities of phenolic compounds," *Journal of Agricultural and Food Chemistry*, vol. 48, no. 8, pp. 3597–3604, 2000.
- [5] S. Berg, M. Bretz, E. M. Hubbermann, and K. Schwarz, "Influence of different pectins on powder characteristics of microencapsulated anthocyanins and their impact on drug retention of shellac coated granulate," *Journal of Food Engineering*, vol. 108, no. 1, pp. 158–165, 2012.
- [6] L. Zhou, H. Wang, J. Yi et al., "Anti-tumor properties of anthocyanins from *Lonicera caerulea* 'Beilei' fruit on human hepatocellular carcinoma: in vitro and in vivo study," *Biomedicine & Pharmacotherapy*, vol. 104, pp. 520–529, 2018.
- [7] Y. Liu, D. Zhang, Y. Wu et al., "Stability and absorption of anthocyanins from blueberries subjected to a simulated digestion process," *International Journal of Food Science and Nutrition*, vol. 65, no. 4, pp. 440–448, 2014.
- [8] C. Czank, A. Cassidy, Q. Zhang et al., "Human metabolism and elimination of the anthocyanin, cyanidin-3-glucoside: a ^{13}C -tracer study," *American Journal of Clinical Nutrition*, vol. 97, no. 5, pp. 995–1003, 2013.
- [9] G. B. Celli, M. S. L. Brooks, and A. Ghanem, "Development and evaluation of a novel alginate-based *in situ* gelling system to modulate the release of anthocyanins," *Food Hydrocolloids*, vol. 60, pp. 500–508, 2016.
- [10] F. U. Amin, S. A. Shah, H. Badshah, M. Khan, and M. O. Kim, "Anthocyanins encapsulated by PLGA@PEG nanoparticles potentially improved its free radical scavenging capabilities via p38/JNK pathway against $\text{A}\beta_{1-42}$ -induced oxidative stress," *Journal of Nanobiotechnology*, vol. 15, no. 1, p. 12, 2017.
- [11] L. Zhao and F. Temelli, "Preparation of anthocyanin-loaded liposomes using an improved supercritical carbon dioxide method," *Innovative Food Science & Emerging Technologies*, vol. 39, pp. 119–128, 2017.
- [12] W. Wang, J. Jung, and Y. Zhao, "Chitosan-cellulose nanocrystal microencapsulation to improve encapsulation efficiency and stability of entrapped fruit anthocyanins," *Carbohydrate Polymers*, vol. 157, pp. 1246–1253, 2017.
- [13] G. Flores, M. L. Ruiz del Castillo, A. Costabile, A. Klee, K. Bigetti Guergoletto, and G. R. Gibson, "In vitro fermentation of anthocyanins encapsulated with cyclodextrins: release, metabolism and influence on gut microbiota growth," *Journal of Functional Foods*, vol. 16, pp. 50–57, 2015.
- [14] T. Zhang, C. Lv, L. Chen, G. Bai, G. Zhao, and C. Xu, "Encapsulation of anthocyanin molecules within a ferritin nanocage increases their stability and cell uptake efficiency," *Food Research International*, vol. 62, pp. 183–192, 2014.
- [15] B. He, J. Ge, P. Yue et al., "Loading of anthocyanins on chitosan nanoparticles influences anthocyanin degradation in gastrointestinal fluids and stability in a beverage," *Food Chemistry*, vol. 221, pp. 1671–1677, 2017.
- [16] V. A. Pereira Jr., I. N. Q. de Arruda, and R. Stefani, "Active chitosan/PVA films with anthocyanins from *Brassica oleracea* (red cabbage) as time-temperature indicators for application in intelligent food packaging," *Food Hydrocolloids*, vol. 43, pp. 180–188, 2015.
- [17] D. Jeong, B. Bae, S. Park, and K. Na, "Reactive oxygen species responsive drug releasing nanoparticle based on chondroitin sulfate-anthocyanin nanocomplex for efficient tumor therapy," *Journal of Controlled Release*, vol. 222, pp. 78–85, 2016.
- [18] M. J. Kim, S. U. Rehman, F. U. Amin, and M. O. Kim, "Enhanced neuroprotection of anthocyanin-loaded PEG-gold nanoparticles against $\text{A}\beta_{1-42}$ -induced neuroinflammation and neurodegeneration via the NF- κB /JNK/GSK3 β signaling pathway," *Nanomedicine: Nanotechnology, Biology and Medicine*, vol. 13, no. 8, pp. 2533–2544, 2017.
- [19] H. Paukkonen, M. Kunnari, P. Laurén et al., "Nanofibrillar cellulose hydrogels and reconstructed hydrogels as matrices for controlled drug release," *International Journal of Pharmaceutics*, vol. 532, no. 1, pp. 269–280, 2017.
- [20] E. M. Ahmed, "Hydrogel: preparation, characterization and applications: a review," *Journal of Advanced Research*, vol. 6, no. 2, pp. 105–121, 2015.
- [21] M. F. Akhtar, M. Hanif, and N. M. Ranjha, "Methods of synthesis of hydrogels ... a review," *Saudi Pharmaceutical Journal*, vol. 24, no. 5, pp. 554–559, 2016.
- [22] J. H. Sung, M. R. Hwang, J. O. Kim et al., "Gel characterisation and *in vivo* evaluation of minocycline-loaded wound dressing with enhanced wound healing using polyvinyl alcohol and chitosan," *International Journal of Pharmaceutics*, vol. 392, no. 1–2, pp. 232–240, 2010.
- [23] K. Swaroop, S. Francis, and H. M. Somashekarappa, "Gamma irradiation synthesis of Ag/PVA hydrogels and its antibacterial activity," *Materials Today: Proceedings*, vol. 3, no. 6, pp. 1792–1798, 2016.
- [24] P. T. Sudheesh Kumar, V. K. Lakshmanan, T. V. Anilkumar et al., "Flexible and microporous chitosan hydrogel/nano ZnO composite bandages for wound dressing: in vitro and in vivo evaluation," *ACS Applied Materials & Interfaces*, vol. 4, no. 5, pp. 2618–2629, 2012.
- [25] B. Singh and L. Pal, "Sterculia crosslinked PVA and PVA-poly(AAm) hydrogel wound dressings for slow drug delivery: mechanical, mucoadhesive, biocompatible and permeability

- properties,” *Journal of the Mechanical Behavior of Biomedical Materials*, vol. 9, pp. 9–21, 2012.
- [26] K. Vimala, Y. M. Mohan, K. S. Sivudu et al., “Fabrication of porous chitosan films impregnated with silver nanoparticles: a facile approach for superior antibacterial application,” *Colloids and Surfaces B: Biointerfaces*, vol. 76, no. 1, pp. 248–258, 2010.
- [27] X. Zhang, W. Cai, L. Hao, S. Feng, Q. Lin, and W. Jiang, “Preparation of Fe_3O_4 /reduced graphene oxide nanocomposites with good dispersibility for delivery of paclitaxel,” *Journal of Nanomaterials*, vol. 2017, Article ID 6702890, 10 pages, 2017.
- [28] N. T. Nguyen and J. H. Liu, “A green method for *in situ* synthesis of poly(vinyl alcohol)/chitosan hydrogel thin films with entrapped silver nanoparticles,” *Journal of the Taiwan Institute of Chemical Engineers*, vol. 45, no. 5, pp. 2827–2833, 2014.
- [29] Y. Yuan, L. Wang, R. J. Mu et al., “Effects of konjac glucomannan on the structure, properties, and drug release characteristics of agarose hydrogels,” *Carbohydrate Polymers*, vol. 190, pp. 196–203, 2018.
- [30] T. W. Chung, T. H. Chou, and K. Y. Wu, “Gelatin/PLGA hydrogel films and their delivery of hydrophobic drugs,” *Journal of the Taiwan Institute of Chemical Engineers*, vol. 60, pp. 8–14, 2016.
- [31] B. Singh, S. Sharma, and A. Dhiman, “Design of antibiotic containing hydrogel wound dressings: biomedical properties and histological study of wound healing,” *International Journal of Pharmaceutics*, vol. 457, no. 1, pp. 82–91, 2013.
- [32] M. Pandima Devi, M. Sekar, M. Chamundeswari et al., “A novel wound dressing material — fibrin–chitosan–sodium alginate composite sheet,” *Bulletin of Materials Science*, vol. 35, no. 7, pp. 1157–1163, 2012.



Hindawi
Submit your manuscripts at
www.hindawi.com

